One Thousand Days of SN2015bn: *HST* Imaging Shows a Light Curve Flattening Consistent with Magnetar Predictions

Matt Nicholl[1,2] , Peter K. Blanchard[1] , Edo Berger[1] , Kate D. Alexander[1] , Brian D. Metzger[3] , Kornpob Bhirombhakdi[4] ,
Ryan Chornock[4], Deanne Coppejans[5], Sebastian Gomez[1] , Ben Margalit[3] , Raffaella Margutti[5] , and Giacomo Terreran[5]

[1] Harvard-Smithsonian Center for Astrophysics, 60 Garden Street, Cambridge, MA, 02138, USA; mrn@roe.ac.uk
[2] Institute for Astronomy, University of Edinburgh, Royal Observatory, Blackford Hill, Edinburgh EH9 3HJ, UK
[3] Department of Physics and Columbia Astrophysics Laboratory, Columbia University, New York, NY 10027, USA
[4] Astrophysical Institute, Department of Physics and Astronomy, 251B Clippinger Lab, Ohio University, Athens, OH 45701, USA
[5] Center for Interdisciplinary Exploration and Research in Astrophysics (CIERA) and Department of Physics and Astronomy,
Northwestern University, Evanston, IL 60208, USA

Abstract

We present the first observations of a Type I superluminous supernova (SLSN) at $\gtrsim 1000$ days after maximum light. We observed SN 2015bn using the *Hubble Space Telescope* (*HST*) Advanced Camera for Surveys in the F475W, F625W and F775W filters at 721 days and 1068 days. SN 2015bn is clearly detected and resolved from its compact host, allowing reliable photometry. A galaxy template constructed from these data further enables us to isolate the SLSN flux in deep ground-based imaging. We measure a light curve decline rate at >700 days of 0.19 ± 0.03 mag$(100\,\mathrm{d})^{-1}$, much shallower than the earlier evolution, and slower than previous SLSNe (at any phase) or the decay rate of ^{56}Co. Neither additional radioactive isotopes nor a light echo can consistently account for the slow decline. A spectrum at 1083 days shows the same [O I] $\lambda 6300$ and [Ca II] $\lambda 7300$ lines as seen at $\sim$300–400 days, with no new features to indicate strong circumstellar interaction. Radio limits with the Very Large Array rule out an extended wind for mass-loss rates $10^{-2.7} \lesssim \dot{M}/v_{10} \lesssim 10^{-1.1}\, M_\odot\,\mathrm{yr}^{-1}$ (where v_{10} is the wind velocity in units of $10\,\mathrm{km\,s}^{-1}$). The optical light curve is consistent with $L \propto t^{-4}$, which we show is expected for magnetar spin-down with inefficient trapping; furthermore, the evolution matches predictions from earlier magnetar model fits. The opacity to magnetar radiation is constrained at $\sim$0.01 cm^2 g^{-1}, consistent with photon-matter pair-production over a broad $\sim$GeV–TeV range. This suggests that the magnetar spectral energy distribution, and hence the "missing energy" leaking from the ejecta, may peak in this range.

Key words: supernovae: general – supernovae: individual (SN2015bn)

1. Introduction

Hydrogen-poor superluminous supernovae (Type I SLSNe; here simply SLSNe) are a rare class of massive star explosions with typical peak absolute magnitudes $M \sim -21$ mag (Chomiuk et al. 2011; Quimby et al. 2011). Despite intense observational and theoretical study, the energy source underlying their light curves has remained uncertain (e.g., Moriya et al. 2018).

Normal stripped-envelope supernovae (SNe) are powered by $\sim$few $\times\,0.1\,M_\odot$ of synthesized ^{56}Ni (e.g., Drout et al. 2011), whereas SLSNe would require several solar masses if that was the primary energy source. Such a large ^{56}Ni mass conflicts with the early light curves (Nicholl et al. 2013), late-time limits (Blanchard et al. 2018), and with spectra (Dessart et al. 2012; Jerkstrand et al. 2017; Nicholl et al. 2018), but a number of SLSNe do fade at a rate that resembles the decay of ^{56}Co, the daughter nucleus of ^{56}Ni (Gal-Yam et al. 2009; De Cia et al. 2018).

The most popular model for SLSNe is the spin-down of a millisecond magnetar with magnetic field $B \gtrsim 10^{13}$ G (Kasen & Bildsten 2010). While this reproduces most SLSN observables (Inserra et al. 2013; Nicholl et al. 2017), a "smoking gun" has proven elusive; thus competing models, such as ejecta interacting with a circumstellar medium (CSM), remain competitive. It was hoped that a magnetar engine could drive an X-ray breakout months after the explosion

(Metzger et al. 2014), but this has not been detected (Inserra et al. 2017; Margutti et al. 2018), and more recent (and realistic) models predict that breakouts should be rare (Margalit et al. 2018).

A more robust test for the magnetar engine comes from the late-time light curve. The spin-down luminosity ultimately follows a power law, $L \propto t^{-\alpha}$, so eventually the decline should become shallower than ^{56}Co decay, which follows an exponential (half-life ≈ 77 days). While many SLSN light curves have been observed to flatten at late times, the spin-down rate can remain within a factor of a few of ^{56}Co decay for hundreds of days (Inserra et al. 2013; Moriya et al. 2017), and most SLSNe are too distant to follow to such late phases.

In this Letter, we report the first detections of a Type I SLSN at $\gtrsim 1000$ days after maximum light. SN 2015bn is a slowly evolving SLSN at $z = 0.1136$, and has been extensively studied at earlier times (Inserra et al. 2016; Nicholl et al. 2016a, 2016b; Jerkstrand et al. 2017; Leloudas et al. 2017). New imaging with the *Hubble Space Telescope* (*HST*) and *Magellan* reveals a marked flattening in the light curve after $\sim$500 days, consistent with a power law, and a decline rate that is now significantly slower than ^{56}Co decay. Spectroscopy and radio follow-up show no signs of circumstellar interaction. After eliminating several other possibilities, we argue that this is best interpreted as the signature of a magnetar engine.
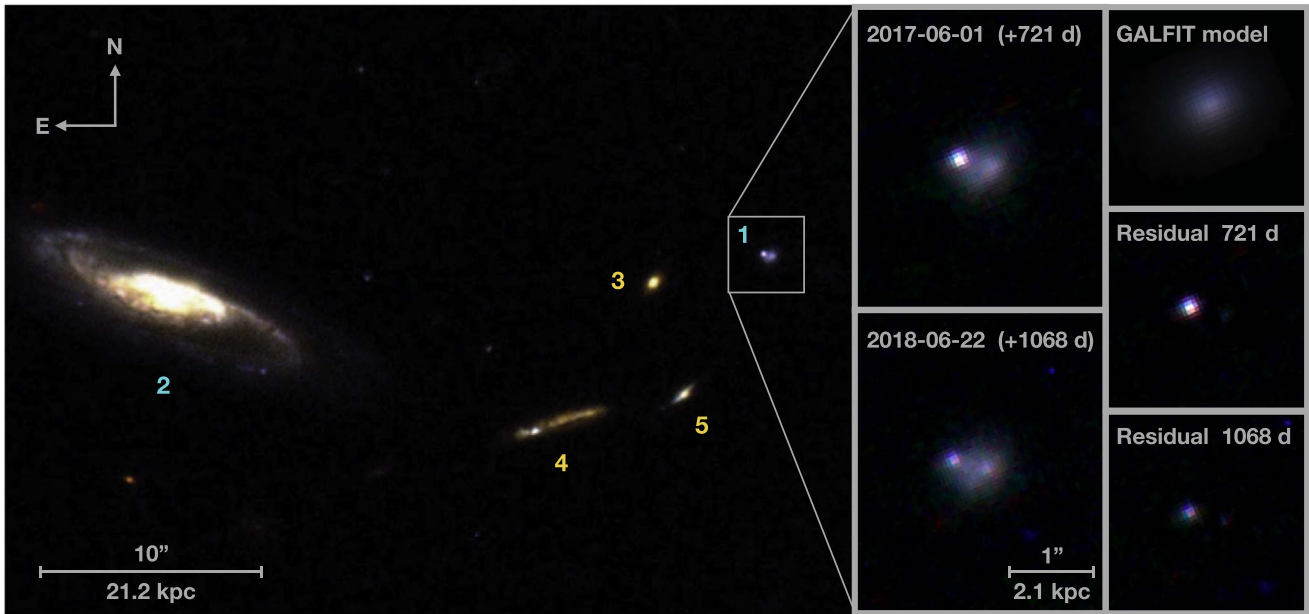
Figure 1. *HST* imaging of SN 2015bn at 721–1068 rest-frame days after maximum. The image on the left is a *gri* three-color composite of the earlier epoch. The host galaxy (labeled 1) and the large spiral (2) are at consistent redshifts, $z \approx 0.11$, with separation and relative magnitudes comparable to the SMC and Milky Way. The other three sources (3–5) are background galaxies at $z \approx 0.35$. Panels on the right show a zoom-in around SN 2015bn and the subtraction of a galaxy model with `galfit`. The SN is clearly detected, fading by a factor ∼2 between observations.

2. Observations

2.1. Optical Imaging

We imaged SN 2015bn using the *HST* Advanced Camera for Surveys Wide Field Channel[6] on 2017-06-01.4 and 2018-06-22.3 (all dates in UT), corresponding to 721 and 1068 days after maximum light in the rest-frame of SN 2015bn. Visits consisted of one orbit per filter in F475W, F625W, and F775W, corresponding closely to *g*, *r*, and *i* bands, where we expect most of the strong emission lines (Nicholl et al. 2016b, 2018; Jerkstrand et al. 2017). Each image contained four dithers in a standard box pattern.

We retrieved the fully processed and drizzled images from the Mikulski Archive for Space Telescopes. Figure 1 shows the combined three-color images. SN 2015bn is clearly visible as a point source superimposed on its host galaxy. We removed the host using a galaxy model constructed with `galfit` (Peng et al. 2002), fitting a Sérsic profile while masking the pixels that were clearly dominated by SN 2015bn. There were no significant differences between the fits obtained in the individual epochs. Subtracting the model from the *HST* images resulted in a clean SN detection with minimal galaxy residuals, as shown in Figure 1. We then performed point-spread function (PSF) photometry with `daophot`, and applied standard zeropoints.[7] We verified that the zeropoints were consistent between the two epochs (to within <0.02 mag) using 16 stars from the Pan-STARRS Data Release 1 catalog (Flewelling et al. 2016).

We obtained ground-based imaging on 2017-02-01.3 and 2018-03-18.7 using the Low Dispersion Survey Spectrograph 3 (LDSS3) on the 6.5-m *Magellan* Clay telescope. Each observation consisted of 10×300 s dithered *r*-band exposures, which we reduced in `pyraf`. From the ground, SN 2015bn appears entirely blended with its (much brighter) host. Subtracting the `galfit` model derived from the *HST* data, after convolving to the ground-based resolution using `hotpants`,[8] we isolated the SN light and performed PSF photometry, determining the zeropoints using the Pan-STARRS catalog.

Our photometry is plotted in Figure 2, along with earlier *g*, *r*, and *i* data from Nicholl et al. (2016a, 2016b). The latest points are fainter than the peak by a factor ≈1500, but a flattening in the light curve beyond ∼500 days is immediately apparent. The new data have been submitted to the Open Supernova Catalog (Guillochon et al. 2017).

2.2. SN Spectroscopy

We observed SN 2015bn spectroscopically on 2018-07-08.9 (1083 rest-frame days after maximum) using LDSS3. The data were reduced in `pyraf`, with flux calibration achieved using a standard star. The spectrum is shown in Figure 3. The mean airmass during the observation was 1.6, and the spectrum redward of ∼7500 Å is contaminated by noise residuals from sky subtraction.

Although the spectrum is dominated by the host, the strongest emission lines from SN 2015bn appear to be visible above the galaxy light. We subtract a model for the host continuum (Nicholl et al. 2016a) and compare to the most recent prior spectrum (at 392 days after maximum; Nicholl et al. 2016b), scaled to match the latest *HST* observations. We find that the broad feature at 6300 Å is consistent with predictions for [O I] λ6300, while a tentative feature at 7300 Å matches [Ca II] λ7300. This indicates that the lines have changed little, despite a gap of 691 days. Our new spectrum likely represents the oldest spectroscopic detection
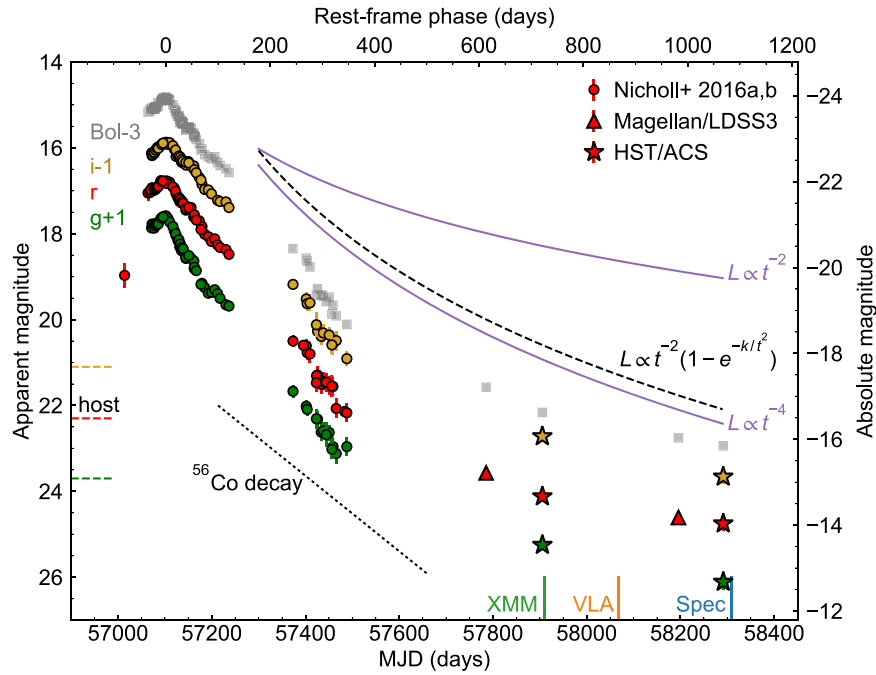
Figure 2. Light curve of SN 2015bn. The points labeled "Bol" are the pseudobolometric magnitudes obtained by integrating the *gri* flux. The absolute scale on the right axis assumes a constant *K*-correction of $-2.5 \log(1 + z)$. Host magnitudes are from SDSS. The decline rate at $\gtrsim 500$ days is much slower than before, and clearly shallower than ^{56}Co decay (dotted line). The post-maximum light curves are broadly consistent with a power law, $L \propto t^{-4}$, equivalent to magnetar spin-down with incomplete thermalization (dashed line). Dates of spectroscopic and radio data (this work), and X-ray data (Bhirombhakdi et al. 2018), are marked, as are host galaxy magnitudes (offset to match light curves).
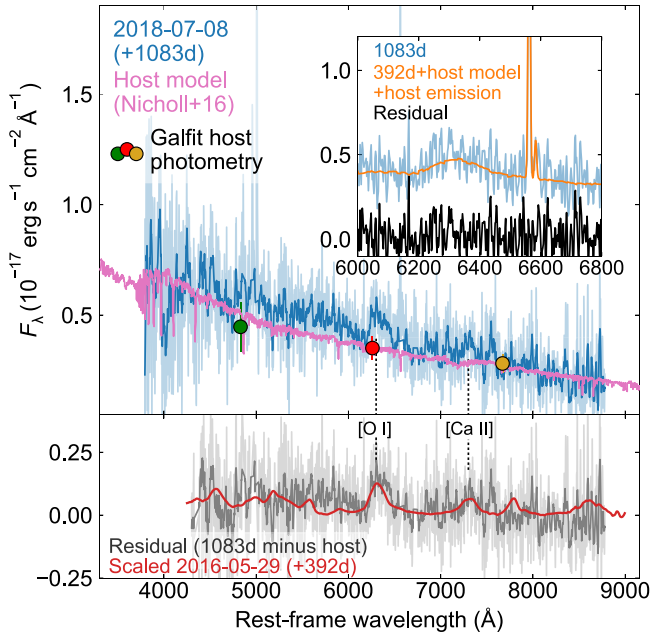
Figure 3. Top: spectrum of SN 2015bn at 1083 days. The spectrum is dominated by galaxy light, and has been scaled to match the host photometry. We have smoothed the data with a Savitsky–Golay filter for clarity. We also plot the model host spectrum from Nicholl et al. (2016a). Bottom: host-subtracted spectrum. Broad features in the residuals match [O I] λ6300 and possibly [Ca II] λ7300. We compare to the spectrum of SN 2015bn at 392 days (Nicholl et al. 2016b), scaled to the latest magnitudes from *HST*. The features in the new spectrum are consistent with the 392 days spectrum, supporting their identification as SN lines Inset: zoom-in around [O I] λ6300 and Hα. The 1083-day spectrum can be modeled as the sum of the host continuum model, the scaled 392 days spectrum, and Gaussian fits to the narrow Hα and [N II] data. Widths have been fixed at the instrumental resolution (8 Å). No broad component to Hα, which would indicate circumstellar interaction (Yan et al. 2017), is observed.

with respect to explosion for any SLSN: the normalized phase is $t/t_d = 13.5$ in the terminology of Nicholl et al. (2018), where $t_d = 80$ days is the decline timescale of the light curve.

2.3. Galaxy Spectroscopy

We also obtained spectra of three galaxies that apparently neighbor SN 2015bn (labeled 3–5 in Figure 1). We find that they are a background group at $z = 0.353$ unrelated to SN 2015bn. The bright ($M_r \approx -21$) spiral galaxy (2) has a spectrum from the Sloan Digital Sky Survey Data Release 7 (Abazajian et al. 2009) that indicates $z = 0.1118$, similar to SN 2015bn.

The relative line-of-sight velocity between this galaxy and the SN host is $c\Delta z = 540\,\mathrm{km\,s^{-1}}$, while their projected separation is $\approx 56\,\mathrm{kpc}$. These values are similar to the Magellanic Clouds relative to the Milky Way, and the absolute magnitude ($M_r = -16.4$), physical size, star formation rate, and metallicity of the host (Nicholl et al. 2016a) are all similar to the SMC. Thus, the host and its bright neighbor appear to be a close analog of the MW-SMC system.

Chen et al. (2017) found that the host of one SLSN, LSQ14mo, was in a likely interacting system with a projected separation of 15 kpc, and proposed that this could increase the likelihood of SLSNe by triggering vigorous star formation. The brightest and bluest pixels in our *HST* images, likely corresponding to the highest star formation rate, actually appear to be on the other side of the galaxy, though we cannot exclude comparable star formation at the position of SN 2015bn until the SLSN has completely faded.

2.4. Radio Observations

We observed SN 2015bn using the Karl G. Jansky Very Large Array (VLA) in B configuration, on 2017 November 10 (867 rest-frame days after maximum).[9] SN 2015bn was not detected to 3σ limiting flux densities of 48 μJy in K band (21.8 GHz) and 63 μJy in Ka band (33.5 GHz).

3. Analysis

The principal discovery from our observations is the shallow light curve beyond 500 days. The mean slope in g, r, i between the *HST* epochs is 0.19 ± 0.03 mag$(100\,\mathrm{d})^{-1}$. Integrating the flux over these bands yields a similar pseudobolometric decline of 0.22 ± 0.02 mag$(100\,\mathrm{d})^{-1}$. This is the slowest decline rate measured for any hydrogen-poor SLSN, and is significantly slower than the 1.43 mag$(100\,\mathrm{d})^{-1}$ during the first 400 days (Nicholl et al. 2016b), and the ^{56}Co decay rate of 0.98 mag$(100\,\mathrm{d})^{-1}$.

Few SLSNe have deep observations at this phase, so it is possible that others reach a similarly slow decline; however, the only other SLSN with photometry at a comparable phase, PTF10nmn, did not show a change in slope up to ≈ 700 days (De Cia et al. 2018). The light curve of PS1-14bj appeared to reach to a slope that is flatter than ^{56}Co by around 400 days (Lunnan et al. 2016), but further monitoring was not available to confirm this. We now examine possible causes of the flattening in SN 2015bn.

3.1. Light Echo?

Light echoes occur when light emitted earlier in the SN evolution is reflected into our line of sight by nearby dust sheets, giving an apparent luminosity boost after a light travel time. For nearby SNe, this is readily identifiable through a change in the spatial emission profile, but at the distance of SN 2015bn, 1 lt-yr corresponds to only $\sim 10^{-4}$ arcsec. An echo beginning ~ 2 years after explosion could roughly match the late-time brightness if it was ≈ 8 mag fainter than the light curve peak. Lunnan et al. (2018) recently detected the first light echo in a H-poor SLSN, iPTF16eh, via a Mg II resonance line.

There are several issues with interpreting the behavior of SN 2015bn as an echo. First, the luminosity of an echo is expected to evolve as t^{-1} (e.g. Graur et al. 2018), which is flatter than what we observe. Second, the spectrum is consistent with a typical SLSN nebular spectrum, whereas an echo should contain features from earlier phases, when the SN was brighter. However, we caution that the spectrum is noisy and dominated by host galaxy light.

Finally, dust is more efficient in reflecting blue light, which changes the observed colors. We measure $g - i = 0.45 \pm 0.24$ at 1068 days, which is consistent with the color at 300 days ($g - i = 0.35 \pm 0.17$) but not with the peak ($g - i = -0.27 \pm 0.02$). A similar finding applies to $g - r$ and $r - i$. We therefore conclude that an echo cannot explain the slow evolution.

3.2. Radioactive Isotopes?

Follow-up of nearby SNe at $\gtrsim 900$ days has revealed evidence for the decay chain ^{57}Ni $\rightarrow$ ^{57}Co $\rightarrow$ ^{57}Fe, in both core-collapse (Seitenzahl et al. 2014) and Type Ia SNe

(Shappee et al. 2017; Graur et al. 2018). While the relative abundance of ^{57}Ni is typically low (^{57}Ni/^{56}Ni $\lesssim 0.05$), the long lifetime of ^{57}Co (half-life ≈ 272 days) means that it eventually comes to dominate over ^{56}Co.

The decay slope for ^{57}Co is 0.28 mag$(100\,\mathrm{d})^{-1}$, which is comparable to our light curve, but still somewhat faster. A small contribution from the slower reaction ^{55}Fe $\rightarrow$ ^{55}Mn (half-life ≈ 1000 days) could help to mitigate this. Seitenzahl et al. (2014) also looked for signatures of ^{60}Co and ^{44}Ti in SN 1987A, but the half-lives of these species are too long (5–60 years) to be relevant to SN 2015bn yet.

The more significant problem for this scenario is that the pseudobolometric luminosity of SN 2015bn at 900 days is $10^{40.8}$ erg s^{-1}, i.e. 400–4000 times greater than SNe Ia at the same phase (Graur et al. 2018). The required ^{57}Co mass is $\gtrsim 6\,M_\odot$. We are not aware of any explosion model capable of producing this; even the most massive pair-instability models from Heger & Woosley (2002) synthesize an order of magnitude less ^{57}Co (while making $40\,M_\odot$ of ^{56}Co). For a solar ratio of ^{57}Co/^{56}Co $= 0.023$ (Lodders 2003), the implied ^{56}Co mass would be $> 260\,M_\odot$.

3.3. Circumstellar Interaction?

Assuming a velocity of ~ 7000 km s^{-1} (Nicholl et al. 2016a, 2016b), we see that the ejecta expand to a radius $\approx 6 \times 10^{16}$ cm within 1000 days, and the fastest ejecta likely reach $\sim 10^{17}$ cm. Yan et al. (2017) found that up to $\sim 15\%$ of SLSNe encounter hydrogen-rich CSM at $\sim 10^{16}$ cm, as indicated by the sudden appearance of broad hydrogen emission lines in their spectra, while Lunnan et al. (2018) identified a circumstellar shell at $\gtrsim 10^{17}$ cm around iPTF16eh from its light echo. Thus, interaction with a massive CSM at a similar radius could be a plausible luminosity source for SN 2015bn.

However, none of the interacting events in Yan et al. (2017) showed a shallow light curve resembling SN 2015bn, though the interaction in those events occurred much earlier (100–250 days) when the SLSNe were ~ 1–2 orders of magnitude brighter. Chen et al. (2018) recently studied SN 2017ens, another SLSN that developed strong and broad Hα emission at $\gtrsim 100$ days, finding its light curve was essentially flat at this phase.

We examine the Hα region of our spectrum in Figure 3. We subtract a model consisting of the scaled 392 days spectrum and a linear host continuum, and fit the Hα and [N II] lines with Gaussian profiles. A satisfactory fit is obtained with the width fixed at the instrumental resolution; i.e., the lines are unresolved, and no broad component is present above the level of the noise. The flux in Hα is 1.6×10^{-16} erg s^{-1} cm^{-2}, consistent with host emission (Nicholl et al. 2016a).

While Hα is generally the strongest line in SNe interacting with hydrogen-rich material, interaction with hydrogen-free material is more difficult to exclude. Ben-Ami et al. (2014) detected narrow [O I] $\lambda 5577$ emission from SN 2010mb, and proposed that it was a signature of interaction. We do not observe this line in SN 2015bn to a limit of $\lesssim 4 \times 10^{37}$ erg s^{-1}, which is ~ 10–100 times fainter than the line in SN 2010mb up to one year after explosion. A possible caveat is that this line is only predicted to be strong at densities $> 10^7$ g cm^{-3}.

Late-onset interaction in other events has been interpreted as a collision with a detached shell, but a slow decline could also result from an extended dense wind. Figure 4 shows predicted radio emission for SNe interacting with winds of different densities

---
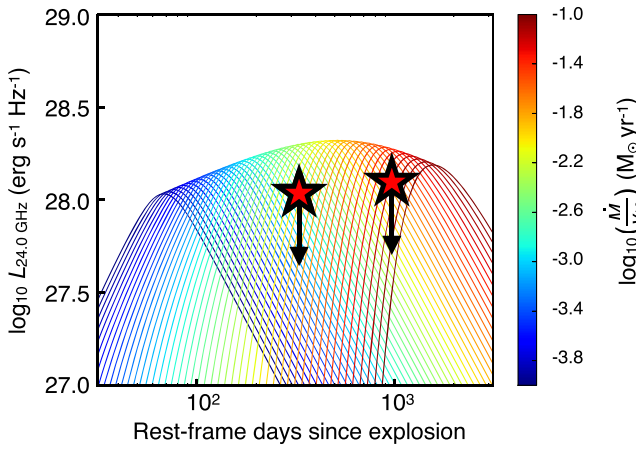
Figure 4. VLA upper limits on the 24 GHz (rest-frame) emission from SN 2015bn. The earlier limit is from Nicholl et al. (2016a). Overplotted are models from Kamble et al. (2016) predicting the radio emission from an SN shock expanding into a circumstellar wind (density $\propto r^{-2}$). The VLA non-detections rule out extended winds corresponding to mass-loss rates of $10^{-2.7} \lesssim \dot{M}/v_{10} \lesssim 10^{-1.1} \, M_\odot \, \mathrm{yr}^{-1}$.

(Kamble et al. 2016), which we compare to our VLA limit and an earlier limit from Nicholl et al. (2016a). Parameterizing the wind mass-loss rate as $\dot{M}/v_{10}$, where v_{10} is the wind velocity in units of $10 \, \mathrm{km \, s^{-1}}$, the combined limits at 1–3 years rule out winds with $10^{-2.7} \lesssim \dot{M}/v_{10} \lesssim 10^{-1.1} \, M_\odot \, \mathrm{yr}^{-1}$. For a typical Wolf–Rayet wind velocity $\sim 1000 \, \mathrm{km \, s^{-1}}$, this corresponds to $10^{-4.7} \lesssim \dot{M} \lesssim 10^{-3.1} \, M_\odot \, \mathrm{yr}^{-1}$, excluding a wind significantly more dense than those from SN Ic progenitors (e.g., Berger et al. 2002; Soderberg et al. 2006; Drout et al. 2016).

Comparing to models for the optical luminosity from Nicholl et al. (2016a), we can rule out most of the parameter space where the light curve peak can be powered by interaction with a dense wind, and also disfavors this as the primary late-time power source.

3.4. Magnetar Spin-down?

The most popular model for SLSNe is a magnetar engine. At late times the engine power decays as $L \propto t^{-\alpha}$; a standard magnetic dipole has $\alpha = 2$. A long-standing prediction is that SLSNe should eventually track this power law. While many SLSN light curves have been observed to flatten with time, late observations have generally been either similar to ^{56}Co decay (Inserra et al. 2013) or of insufficient signal-to-noise ratio (Lunnan et al. 2016) to make strong statements.

In Figure 2, we plot representative curves for $\alpha = 2$ and $\alpha = 4$. The best-fitting power law at 200–1100 days has $\alpha \approx 3.8$, steeper than a standard dipole. However, it is expected that the energy available from spin-down is not completely thermalized at late times; assuming that this energy is injected primarily as high-energy photons, the optical depth in the expanding ejecta decreases with time as $\tau \propto t^{-2}$ (Wang et al. 2015; Chen et al. 2015). Including this "leakage" term gives

$$L \propto t^{-2}(1 - e^{-kt^{-2}}) \approx kt^{-4}, \qquad (1)$$

where $k = 3\kappa_\gamma M_{\mathrm{ej}}/(4\pi v_{\mathrm{ej}}^2)$ is the trapping coefficient, M_{ej} and v_{ej} are the mass and velocity of the ejecta and κ_γ is the opacity to high-energy photons. The second equality comes from a Taylor expansion applicable at late times. Thus a realistic
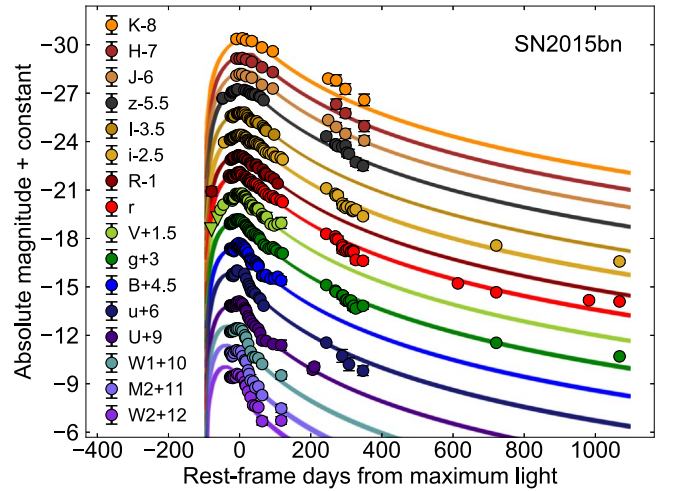
Figure 5. Fit to the complete ultraviolet-optical-near-infrared light curves of SN 2015bn with the magnetar model in mosfit (Guillochon et al. 2018). The fit and derived parameters are essentially unchanged compared to those in Nicholl et al. (2017), and naturally account for the new late-time data.

power law is not $\alpha = 2$, but rather $\alpha \approx 4$, close to what we observe.

We model the full light curve of SN 2015bn using mosfit (Guillochon et al. 2018). SN 2015bn has previously been fit using this code and a magnetar model by Nicholl et al. (2017), who described the methodology. The result is shown in Figure 5. Given that new data comprise only $\approx 1\%$ of the total light curve points, it is unsurprising that the fit is unchanged with respect to Nicholl et al. (2017). We find a spin period $P/\mathrm{ms} = 2.32 \pm 0.22$, magnetic field $\log(B/10^{14}\mathrm{G}) = -0.51 \pm 0.09$, and ejecta mass $\log(M_{\mathrm{ej}}/M_\odot) = 1.04 \pm 0.03$. More interesting is that the best fit to the first 400 days gave a reasonably accurate prediction of the evolution at >1000 days. The model matches the data at 721 days, and agrees to better than a factor two at 1083 days, though the later data appear systematically above the fit. The previous modeling suggested $\kappa_\gamma \sim 0.01 \, \mathrm{cm^2 \, g^{-1}}$, which we confirm here.

3.4.1. Is There a "Missing Energy Problem"?

The requirement for inefficient trapping has important implications. Our model implies that by ~ 700 days the engine is injecting $\sim 10^{43} \mathrm{erg \, s^{-1}}$, but only a few percent are thermalized, indicating a large fraction of "missing energy" escaping. Bhirombhakdi et al. (2018) imaged SN 2015bn in soft X-rays at 725 days. They detected no flux at 0.3–10 keV to a limit of $\lesssim 10^{41} \mathrm{erg \, s^{-1}}$, prompting them to conclude that $\lesssim 1.5\%$ of the magnetar input escapes in this range. The energy does not escape in the radio either; using our derived parameters from mosfit, Margalit et al. (2018) predicted that the ejecta will remain optically thick to free–free absorption at ~ 20–$40 \, \mathrm{GHz}$ for approximately 10 years, consistent with our VLA non-detections.

Metzger et al. (2014) described how the magnetar should inflate a nebula of energetic particles and radiation. When the nebula is initially "compact," photon–photon pair creation gives a relatively flat spectral energy distribution (SED) with an upper cut-off at ~ 1–10 MeV. Using their Equation (13) and our parameters from mosfit, we find a dimensionless compactness parameter $\ell \lesssim 1$ by maximum light and $\ell \sim 0.002$ at the timescales that we probe here. At low compactness, the SED

cut-off moves up to the GeV–TeV range. The dominant opacity is then from photon-matter pair creation, which has an opacity $\kappa_\gamma \sim 0.01$–$0.03\,\mathrm{cm^2\,g^{-1}}$ over many orders of magnitude in energy (Zdziarski & Svensson [1989]). The fact that the value of κ_γ inferred from optical data agrees with this range may provide indirect evidence that the magnetar SED is peaking in high-energy gamma-rays, and that the escape of this radiation is the source of missing energy. Renault-Tinacci et al. ([2018]) searched for GeV leakage from SLSNe with *Fermi*, but their limits were not deep enough to detect $\sim 10^{43}\,\mathrm{erg\,s^{-1}}$, leaving open this possibility.

3.5. Freeze-out?

The mechanisms discussed in Sections [3.2]–[3.4] assume that energy deposition is instantaneous. However, if the heat source is coupled to the ejecta through ionization and recombination, this assumption holds only if the recombination timescale is shorter than the heating timescale, which may not be true at late times when the ejecta density is low. This process of "freeze-out" can result in a light curve tracking the recombination rate instead of the heating rate (Fransson & Kozma [1993]; Fransson & Jerkstrand [2015]).

Following Kerzendorf et al. ([2017]) and Graur et al. ([2018]), we parameterize freeze-out as a luminosity source that evolves as t^{-3} (i.e., in proportion to the density, assuming constant expansion). Graur et al. ([2018]) defined $t_{\mathrm{freeze},50}$ as the time when freeze-out accounts for half of the emission. If freeze-out dominates by ~ 700 days, we find $t_{\mathrm{freeze},50} \sim 400$ days. This is much earlier than in SN 1987A and a number of nearby SNe Ia, for which the timescales are typically $\gtrsim 800$ days (Fransson & Kozma [1993]; Graur et al. [2018]). It therefore seems unlikely that freeze-out alone can account for the flattening, but more detailed modeling is required here.

4. Discussion and Conclusions

We have presented optical imaging, spectroscopy, and deep radio limits for SN 2015bn at ≈ 700–1100 days after maximum light. *HST* images enabled us to localize the faint SN within its compact host, and reliably extract its flux. We found a significant flattening in the light curve, which is now much slower than ^{56}Co decay, while the spectrum remains consistent with previous observations at ~ 300 days.

We showed that the spectrum, colors, and decline rate were inconsistent with a light echo. The luminosity, $\sim 10^{41}\,\mathrm{erg\,s^{-1}}$, is too large for slowly decaying radioactive isotopes like ^{57}Co; the required $\gtrsim 6\,M_\odot$ far exceeds any physical model of which we are aware. Late-time circumstellar interaction is a more plausible mechanism to slow the light curve; however, neither the spectrum nor radio data indicate interaction. In particular, SN 2015bn lacks the broad Hα seen in other SLSNe that interact at late times (Yan et al. [2017]).

The light curve shape can be reproduced with a power law, $\alpha \approx 4$, which we show is expected for a magnetar engine with incomplete trapping. In fact, the same magnetar parameters inferred from earlier data naturally predict an evolution in reasonable agreement with our observations. Our fit suggests that only a few percent of the $\sim 10^{43}\,\mathrm{erg\,s^{-1}}$ input is thermalized at this phase, suggesting significant luminosity from leakage at other wavelengths. However, our radio data, and soft X-ray data from Bhirombhakdi et al. ([2018]), have yielded non-detections. The opacity to magnetar input inferred from our

light curve modeling, $\sim 0.01\,\mathrm{cm^2\,g^{-1}}$, suggests a harder spectrum, likely concentrated at $\gg 10\,\mathrm{MeV}$, which may be where the missing energy is escaping.

While SN 2015bn is the first SLSN observed to reach a decline much shallower than ^{56}Co decay, there is a recent example of a SN Ic, iPTF15dtg, exhibiting similar behavior. Taddia et al. ([2018]) interpreted this as a signature of magnetar powering. We note that the nebular spectrum of iPTF15dtg closely resembles SN 2015bn, and shows several features, such as prominent O I $\lambda 7774$ and [O III] $\lambda 5007$, which are more characteristic of SLSNe than normal SNe Ic (Milisavljevic et al. [2013]; Nicholl et al. [2016b], [2018]).

The strength of any [O III] emission in our latest spectrum is difficult to establish given the low signal-to-noise ratio; however, it is clearly weaker than the line we identify as [O I]. This is interesting given that (Chevalier & Fransson [1992]) find that in a pulsar-energized SN at this phase, [O III] should often be the strongest line. Following their discussion, the high ratio of [O I]/[O III] could indicate a large ejecta mass, such that the highly ionized region does not extend too far in mass coordinate (Metzger et al. [2014]), and/or significant clumping (a density enhancement $\gtrsim 10$), which can boost the [O I] emission (see also Jerkstrand et al. [2017]).

The latest photometry of SN 2015bn, at 1068 days, is slightly brighter than the predictions of the basic magnetar model. While we caution that this is based on only two epochs, such an effect could be interpreted as evidence that the power law is not exactly $\alpha = 2$, e.g., Metzger et al. ([2018]) have shown that accretion onto a magnetar can alter its spin-down. Alternatively, low-level interaction may be a factor, perhaps connected to earlier undulations in the light curve (Nicholl et al. [2016a]; Inserra et al. [2017]). Finally, we cannot exclude a small contribution from freeze-out effects.
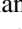
Obtaining observations of additional nearby SLSNe at $\gtrsim 500$ days will be required to determine if the slow decline observed in SN 2015bn is ubiquitous, and whether it is indeed the long-awaited smoking gun for the magnetar. The closest events may hold further promise for detecting leakage of the input energy, and directly probing the engine SED; we suggest such searches should focus on hard X-rays and gamma-rays.

ORCID iDs

Matt Nicholl ● https://orcid.org/0000-0002-2555-3192
Peter K. Blanchard ● https://orcid.org/0000-0003-0526-2248
Edo Berger ● https://orcid.org/0000-0002-9392-9681
Kate D. Alexander ● https://orcid.org/0000-0002-8297-2473
Brian D. Metzger ● https://orcid.org/0000-0002-4670-7509
Kornpob Bhirombhakdi ● https://orcid.org/0000-0003-0136-1281
Sebastian Gomez ● https://orcid.org/0000-0001-6395-6702
Ben Margalit ● https://orcid.org/0000-0001-8405-2649
Raffaella Margutti ● https://orcid.org/0000-0003-4768-7586

References

Abazajian, K. N., Adelman-McCarthy, J. K., Agüeros, M. A., et al. 2009, ApJS, 182, 543
Ben-Ami, S., Gal-Yam, A., Mazzali, P. A., et al. 2014, ApJ, 785, 37
Berger, E., Kulkarni, S., & Chevalier, R. 2002, ApJL, 577, L5
Bhirombhakdi, K., Chornock, R., Margutti, R., et al. 2018, ApJ, submitted (arXiv:1809.02760)
Blanchard, P. K., Nicholl, M., Berger, E., et al. 2018, ApJ, 865, 9
Chen, T.-W., Inserra, C., Fraser, M., et al. 2018, arXiv:1808.04382
Chen, T.-W., Nicholl, M., Smartt, S., et al. 2017, A&A, 602, A9
Chen, T.-W., Smartt, S. J., Jerkstrand, A., et al. 2015, MNRAS, 452, 1567
Chevalier, R. A., & Fransson, C. 1992, ApJ, 395, 540
Chomiuk, L., Chornock, R., Soderberg, A., et al. 2011, ApJ, 743, 114
De Cia, A., Gal-Yam, A., Rubin, A., et al. 2018, ApJ, 860, 100
Dessart, L., Hillier, D. J., Waldman, R., Livne, E., & Blondin, S. 2012, MNRAS, 426, L76
Drout, M., Milisavljevic, D., Parrent, J., et al. 2016, ApJ, 821, 57
Drout, M. R., Soderberg, A. M., Gal-Yam, A., et al. 2011, ApJ, 741, 97
Flewelling, H., Magnier, E., Chambers, K., et al. 2016, arXiv:1612.05243
Fransson, C., & Jerkstrand, A. 2015, ApJL, 814, L2
Fransson, C., & Kozma, C. 1993, ApJL, 408, L25
Gal-Yam, A., Mazzali, P., Ofek, E., et al. 2009, Natur, 462, 624
Graur, O., Zurek, D. R., Rest, A., et al. 2018, ApJ, 859, 79
Guillochon, J., Nicholl, M., Villar, V. A., et al. 2018, ApJS, 236, 6
Guillochon, J., Parrent, J., Kelley, L. K., & Margutti, R. 2017, ApJ, 835, 64
Heger, A., & Woosley, S. 2002, ApJ, 567, 532
Inserra, C., Bulla, M., Sim, S., & Smartt, S. 2016, ApJ, 831, 79
Inserra, C., Nicholl, M., Chen, T.-W., et al. 2017, MNRAS, 468, 4642
Inserra, C., Smartt, S., Jerkstrand, A., et al. 2013, ApJ, 770, 128
Jerkstrand, A., Smartt, S. J., Inserra, C., et al. 2017, ApJ, 835, 13
Kamble, A., Margutti, R., Soderberg, A. M., et al. 2016, ApJ, 818, 111
Kasen, D., & Bildsten, L. 2010, ApJ, 717, 245
Kerzendorf, W., McCully, C., Taubenberger, S., et al. 2017, MNRAS, 472, 2534
Leloudas, G., Maund, J. R., Gal-Yam, A., et al. 2017, ApJL, 837, L14
Lodders, K. 2003, ApJ, 591, 1220
Lunnan, R., Chornock, R., Berger, E., et al. 2016, ApJ, 831, 144
Lunnan, R., Chornock, R., Berger, E., et al. 2018, ApJ, 852, 81
Lunnan, R., Fransson, C., Vreeswijk, P., et al. 2018, arXiv:1808.04887
Margalit, B., Metzger, B. D., Berger, E., et al. 2018, MNRAS, 481, 2406
Margutti, R., Chornock, R., Metzger, B., et al. 2018, ApJ, 864, 45
Metzger, B. D., Beniamini, P., & Giannios, D. 2018, ApJ, 857, 95
Metzger, B. D., Vurm, I., Hascoët, R., & Beloborodov, A. M. 2014, MNRAS, 437, 703
Milisavljevic, D., Soderberg, A. M., Margutti, R., et al. 2013, ApJL, 770, L38
Moriya, T. J., Chen, T.-W., & Langer, N. 2017, ApJ, 835, 177
Moriya, T. J., Sorokina, E. I., & Chevalier, R. A. 2018, SSRv, 214, 59
Nicholl, M., Berger, E., Blanchard, P. K., Gomez, S., & Chornock, R. 2018, arXiv:1808.00510
Nicholl, M., Berger, E., Margutti, R., et al. 2016b, ApJL, 828, L18
Nicholl, M., Berger, E., Smartt, S. J., et al. 2016a, ApJ, 826, 39
Nicholl, M., Guillochon, J., & Berger, E. 2017, ApJ, 850, 55
Nicholl, M., Smartt, S. J., Jerkstrand, A., et al. 2013, Natur, 502, 346
Peng, C. Y., Ho, L. C., Impey, C. D., & Rix, H.-W. 2002, AJ, 124, 266
Quimby, R. M., Kulkarni, S., Kasliwal, M. M., et al. 2011, Natur, 474, 487
Renault-Tinacci, N., Kotera, K., Neronov, A., & Ando, S. 2018, A&A, 611, A45
Seitenzahl, I. R., Timmes, F., & Magkotsios, G. 2014, ApJ, 792, 10
Shappee, B., Stanek, K., Kochanek, C., & Garnavich, P. 2017, ApJ, 841, 48
Soderberg, A. M., Chevalier, R. A., Kulkarni, S. R., & Frail, D. A. 2006, ApJ, 651, 1005
Taddia, F., Sollerman, J., Fremling, C., et al. 2018, arXiv:1806.10000
Wang, S., Wang, L., Dai, Z., & Wu, X. 2015, ApJ, 799, 107
Yan, L., Lunnan, R., Perley, D., et al. 2017, ApJ, 848, 6
Zdziarski, A. A., & Svensson, R. 1989, ApJ, 344, 551